ACS Catalysis

Research Article

pubs.acs.org/acscatalysis

Amine Oxidation Mediated by *N*-Methyltryptophan Oxidase: Computational Insights into the Mechanism, Role of Active-Site Residues, and Covalent Flavin Binding

Bora Karasulu and Walter Thiel*

Max-Planck-Institut für Kohlenforschung, Kaiser-Wilhelm-Platz 1, 45470 Mülheim, Germany

Supporting Information

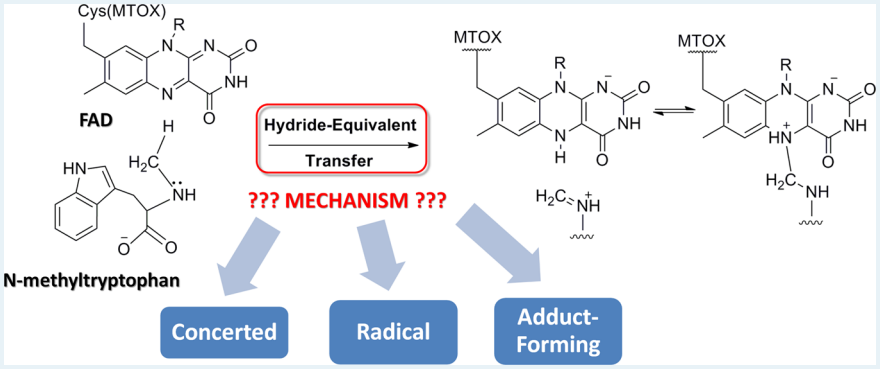

ABSTRACT: Amine oxidation, a process widely utilized by flavoprotein oxidases, is the rate-determining step in the three-step demethylation of *N*-methyltryptophan (NMT) catalyzed by *N*-methyltryptophan oxidase (MTOX), which employs a covalently bound flavin adenine dinucleotide (FAD) as cofactor. For the required transfer of a hydride ion equivalent, three pathways (direct/concerted, radical, and adduct-forming/polar nucleophilic) have been proposed, without a consensus on which one is commonly used by amine oxidases. We combine theoretical pK_a analysis, classical molecular dynamics (MD) simulations, and pure quantum mechanics (QM) and hybrid QM/molecular mechanics (QM/MM) calculations to provide molecular-level insights into the catalytic mechanism of NMT oxidation and to analyze the role of MTOX active-site residues and covalent FAD incorporation for NMT binding and oxidation. The QM(B3LYP-D2/6-31G(d))/CHARMM results clearly favor a direct concerted hydride transfer (HT) mechanism involving anionic NMT as the reactive species. On the basis of classical canonical MD simulations and QM/MM calculations of wild-type MTOX and two mutants (K341Q and H263N), we propose that the K341 residue acts as an active-site base and electrostatically, whereas H263 and Tyr249 only support substrate alignment. Covalent FAD binding leads to a more bent isoalloxazine moiety, which facilitates the binding of anionic NMT but increases the catalytic activity of FAD only slightly.

KEYWORDS: *flavin adenine dinucleotide (FAD), N-methyltryptophan (NMT), biocatalysis, quantum mechanics/molecular mechanics (QM/MM), molecular dynamics, flavoprotein oxidase*

INTRODUCTION

N-Methyltryptophan oxidase (MTOX) catalyzes the oxidative demethylation of a modified amino acid, *N*-methyl-L-tryptophan (*N*-methyltryptophan, NMT), which yields tryptophan, formaldehyde, and hydrogen peroxide as products. Although MTOX can also act on other similar amines (sarcosine, carbinol amines, and thioglycolate), it displays the highest activity with its genuine substrate, NMT (k_{cat} = 4600 min^{-1} and $k_{cat,app}$ = 990 min^{-1}).[1,2] MTOX is a member of the amine oxidase family that also includes monomeric sarcosine oxidase (MSOX), heterotetrameric sarcosine oxidase (TSOX), pipecolare oxidase (PIPOX), and fructosyl amino acid oxidase. Among the members of this family, MTOX shares the highest structural homology (43% sequence identity) with MSOX[3] that is, allegedly, the best characterized member of this family.[4] MTOX and MSOX possess highly analogous reactive pockets. Like all members in this family, they covalently bind a flavin through a conserved cysteine residue (MTOX/MSOX: Cys308/Cys315).[2] Both MTOX and MSOX contain a flavin adenine dinucleotide (FAD) in the form of a covalently bound [8α-(*S*-cysteinyl)FAD] complex. The covalent linkage prevents premature dissociation of an oxidized FAD from MSOX, prior to amine oxidation.[4] Along with the highly electropositive arrangement of the immediate protein environment (containing highly basic residues), the covalent binding of FAD has been proposed to afford a sizable enhancement of the reduction

Received: October 31, 2014
Revised: January 10, 2015
Published: January 13, 2015

DOI: 10.1021/cs501694q
ACS Catal. 2015, 5, 1227−1239

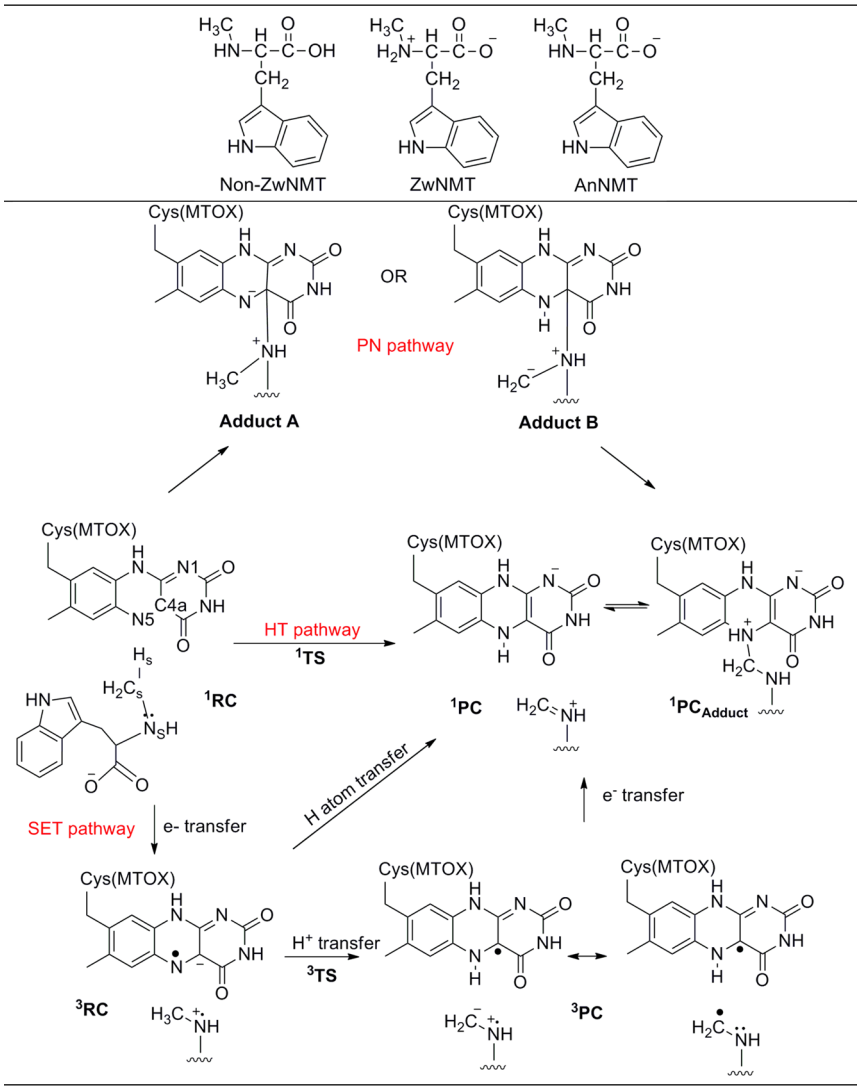

Figure 1. (top) Three forms of *N*-methyltryptophan (NMT): nonzwitterionic (Non-ZwNMT), zwitterionic (ZwNMT), and anionic (AnNMT). (bottom) Polar nucleophilic (PN), direct hydride transfer (HT), and radical (SET) pathways proposed for the amine oxidation step of NMT demethylation catalyzed by MTOX, shown for AnNMT as a representative substrate. In the bottom panel, middle left, labels are included for mechanistically relevant atoms. Abbreviations: RC/PC, reactant/product complex; TS, transition state.

potential of FAD (estimated to ca. 120 mV) in comparison to the noncovalently bound counterparts.[4,5]

Studies on the pH-dependent activity and absorption spectroscopy of MTOX[6,7] and MSOX[8] indicate binding of the substrate in a less reactive neutral form (as zwitterionic or nonzwitterionic species, ZwNMT and Non-ZwNMT; see Figure 1), which is dominant in solution at pH 8.0. Given the optimum working conditions of MTOX (pH 8.0),[1] the substrate NMT is likely ionized within the protein environment by an active-site base to yield the more reactive anionic form (AnNMT; Figure 1). Anionic NMT forms a charge transfer (CT) complex with an oxidized flavin that serves as charge acceptor.[6−8] This complex is thought to be stabilized by pairs of basic residues (MSOX/MTOX: R49/R48-K265/K259 and R52/R51-K348/K341 on the *Si* and *Re* faces of flavin, respectively).[4,8] The deprotonation is believed to occur after binding in the reactive pocket and before the rate-determining C−H cleavage.[7] Two active-site residues in MSOX (Tyr317 and His269) were considered to act as base, but this could be ruled out through mutagenesis studies.[9,10] Deprotonation in MSOX could occur via a putative proton relay system involving N5 of FAD, conserved K265 (homologous to K259 in MTOX), and several nearby water molecules.[9,11] However, K259 mutation in MTOX yielded only a 60-fold rate decrease in the reductive half-reaction, compared with a 2300-fold decrease in the reaction of fully reduced flavin with oxygen, and hence K259 was assigned as the main oxygen activation site.[6] Considering the strong basic properties and the close proximity to FAD-N5 and the backbone of NMT, the K341/K348 residues (MTOX/MSOX) are promising candidates for this role, in line with the almost complete loss of amine oxidation activity in corresponding mutants of MTOX (K341Q, K341R, and K341L).[2]

Catalytic Mechanisms for Oxidative Demethylation of Amines. In general, amine demethylation involves the removal of a methyl group from the N terminus of a given amine substrate via a redox process. Shi et al.[12] proposed a three-step catalytic mechanism for histone (H3K4met) demethylation that can be generalized to amine demethylation mediated by other flavoenzyme oxidases. The first step is the activation or

DOI: 10.1021/cs501694q
ACS Catal. 2015, 5, 1227−1239

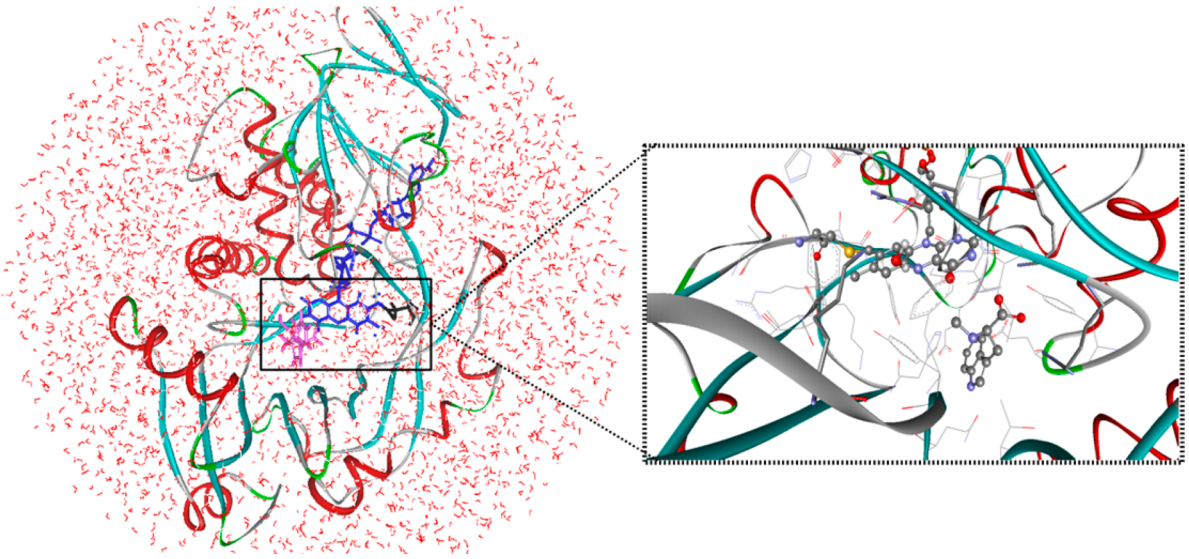

Figure 2. Representative snapshot of the simulation system before the MD simulations: FAD, Cys308, and substrate NMT are shown in stick representations in blue, black, and purple, respectively. In the enlarged active-site view, the atoms in the ball-and-stick representation are colored according to atom type (gray, carbon; white, hydrogen; blue, nitrogen; red, oxygen; yellow, sulfur).

cleavage of the α-CH bond in the methyl group of the amine substrate, followed by an oxidation via transfer of a hydride equivalent. Primary deuterium isotope studies indicate that the cleavage of the chemically inert α-CH bond is the rate-limiting step in different amine oxidases.[7,13] Amine oxidation leads to a two-electron reduction of the flavin (FAD in MTOX), which is then (in an oxidative half-reaction) reoxidized by molecular oxygen, with formation of hydrogen peroxide. This reoxidation is a complementary process that proceeds with very high rates,[6,14] presumably via a modified ping-pong mechanism in MTOX.[15] In the subsequent two steps of demethylation, the formed iminium intermediate is hydrolyzed, and the resulting carbinol amine spontaneously rearranges to yield formaldehyde and the demethylated amine.

The rate-limiting first step of amine demethylation requires the transfer of a hydride equivalent from the amine substrate to FAD. The two electrons and the proton can be transferred in different order, which gives rise to several possible mechanisms: namely, a direct hydride transfer (HT), a radical mechanism via single-electron transfer (SET),[16−18] and an adduct-forming polar nucleophilic mechanism.[19] These mechanisms are depicted in Figure 1 for the case of anionic NMT oxidation. The simplest one is the direct concerted transfer of the two electrons and the proton as a hydride anion from the α-carbon atom of the substrate to FAD. In the radical and adduct-forming mechanisms, there are intermediate species.

Numerous published studies favor different mechanisms for different amine oxidases (see refs 20−25 for comprehensive reviews). ^{15}N kinetic isotope effect measurements and computations on MTOX did not provide clear support for either the HT or SET mechanism.[7,26] The SET mechanism was supported on the basis of cyclopropyl inhibitor studies on LSD1,[27] but this was later challenged[13] by virtue of the fact that some other flavoprotein oxidases, for which hydride transfer is considered the most likely mechanism, are also inactivated by cyclopropyl inhibitors.[28,29] The absence of any conceivable intermediate (i.e., a flavin or amine radical species) in kinetic, EPR, ENDOR, and other spectroscopic studies on MTOX[1,30] as well as other amine oxidases[11,13,31] was proposed to support the HT mechanism. However, the failure to detect any intermediates was considered to be inconclusive by others,[16,26] in view of the following scenario. The initial SET process could be reversible but not rate-limiting, with the back-transfer being much faster, which would lead to low concentrations of the short-lived radical intermediates that could be undetectable by experimental techniques.

These conflicting experimental findings on the catalytic mechanism of an amine oxidation call for a theoretical study to unravel molecular-level details that are not directly observable in experiments. Among the published computational studies on amine oxidases, only a few cover some aspects within the scope of the current work. A pure quantum mechanical (QM) investigation on MTOX-mediated amine oxidation addressed a simple model system consisting of a truncated isoalloxazine moiety of the flavin and dimethylamine ($NH(CH_3)_2$) as the substrate.[26] The computed DFT(B3LYP) energies were found to favor the direct hydride mechanism over the radical-SET mechanism for MTOX.[26] Another QM-only DFT(M06-2X) investigation was carried out[32] on monoamine oxidase (MAO), which binds FAD covalently through a cysteine residue. Vianello et al.[32] proposed a two-step hydride transfer scheme as the working mechanism for MAO-B, involving an adduct between reduced flavin and the imine species resulting from the transfer of a hydride equivalent. QM/molecular mechanical (QM/MM) studies on enzymatic demethylation are still missing for MTOX, but a few are available for other similar flavoprotein amine oxidases. In recent QM/MM work,[33] we addressed lysine-specific demethylase 1 (LSD1), an oxidase that binds a FAD noncovalently and works with aliphatic methyllysine substrates. Direct hydride transfer was shown to be the most feasible mechanism in LSD1, the formation of the imine-FAD adduct was confirmed (through a N5−C4a bond, similar to the situation in MAO[32]), and the lysine residue in the conserved Lys-H_2O-N5 motif (K661, analogous to K259 in MTOX) was identified as the active-site base responsible for ionizing the protonated substrate. Another recent QM/MM study considered human MAO-B with benzylamine as substrate

DOI: 10.1021/cs501694q
ACS Catal. 2015, 5, 1227−1239

and supported a concerted asynchronous polar nucleophilic mechanism.[34]

In this article, we report the results from classical MD simulations as well as QM-only and QM/MM calculations on the amine oxidation step of *N*-methyltrytophan demethylation mediated by MTOX. The objective is to probe the catalytic mechanism in the amine oxidation step and to gain detailed molecular-level insight into the role of the active-site MTOX residues. We elaborate on the role of H263 and K341 as potential active-site bases that may ionize the enzyme−substrate complex. We complete our discussion by addressing the role of covalent binding of the cofactor FAD during substrate binding and amine oxidation.

COMPUTATIONAL METHODOLOGY

The simulations reported here are based on the currently only available crystal structure of MTOX (PDB code 2UZZ[2]) from *Escherichia coli* in complex with FAD, which is covalently bound via Cys308 and acts as an oxidative agent for NMT. The crystal structure lacks crystal water molecules due to its low resolution, 3.2 Å, and does not contain a substrate (NMT) in the active site. Therefore, the substrate was modeled into the binding pocket through flexible docking procedures using Vina[35] (see the Supporting Information for further details). The docking of NMT resulted in a structure with a good binding affinity (−7.6 kcal/mol), which agrees well with the proposed structural model for NMT in MTOX (prepared using dimethylglycine in MSOX as template)[2] in terms of H-bonding and π−cation interactions. In addition, one crucial water molecule was added manually, which forms the conserved Lys-H_2O-N5 motif proposed for MTOX[6] and other similar oxidases (such as MSOX[36]). The simulation system consisted of ca. 18000 atoms (see Figure 2). It was neutralized and solvated in a water droplet (with a radius of 35 Å around the center of mass of its main components: substrate, flavin, and enzyme) in analogy to our previous study.[33] More detailed information on the setup procedure is given in the Supporting Information.

The classical MD simulations were performed with CHARMM[37] at a constant temperature (300 K) using a time step of 1 fs. The MD production runs were long enough (20 ns) to provide good starting points for the subsequent QM/MM calculations. The MM force field parameters for the three forms of the nonstandard NMT substrate were prepared by modifying the standard Trp parameters. Force field parameters for FAD were adopted from the literature[38] and modified to account for the covalent binding of Cys308 at the C8-methyl position. CHARMM22 parameters[39] and the TIP3P model[40] were used for all standard residues and for water molecules, respectively. The protonation states of the protein residues at the optimal pH of MTOX (pH 8.0)[1] were determined with the PROPKA software.[41]

QM-only calculations were carried out using density functional theory (DFT) and the Gaussian09 program suite.[42] For benchmarking purposes, four different functionals (B3LYP[43] and B3LYP-D2 with Grimme-type dispersion corrections,[44] M06-2X,[45] LC-ωPBE,[46] and ωB97xD[47]) were utilized in combination with the 6-31G(d) or TZVP basis set. Geometry optimizations and the following vibrational analysis were done either in the gas phase or in water described by an implicit solvent model (CPCM[48]), without any constraints in the optimizations. Intrinsic reaction coordinate (IRC) calculations were used for locating the reactant and product complexes (RC and PC), starting from the transition state (TS) connecting them.

Hybrid QM/MM studies of the full simulation system were performed with the ChemShell program suite.[49] The QM part of the system was treated at the DFT level (B3LYP-D2 with Grimme-type dispersion corrections[44]) using Gaussian09. The MM calculations were handled by the DL_POLY code[50] implemented in ChemShell using the aforementioned force-field parameters. The QM/MM treatment employed electrostatic embedding in combination with the charge-shift scheme,[51] and the atoms at the QM/MM boundary were treated by the link-atom approach.[49] QM/MM geometry optimizations were carried out with the hybrid delocalized internal coordinate (HDLC) optimizer[52] implemented in ChemShell. Starting geometries for optimizations were taken from several snapshots of the canonical MD ensembles, and only residues within 15 Å of FAD were optimized in order to reduce the computational burden and also to retain the overall protein structure. The optimized structures were subject to numerical force constant calculations in ChemShell to determine the vibrational modes and to characterize the optimized stationary points (i.e., one single negative eigenvalue of the corresponding Hessian matrix for TS, none for minima). Gibbs free energies (ΔG) and other thermodynamic properties were evaluated using the standard rigid-rotor harmonic-oscillator approximation. Theoretical reaction rates were approximated from the relevant Gibbs free energy barrier $\Delta G^{\ddagger}$ (the free energy of activation) in the usual manner using the Arrhenius equation.

In both QM-only and QM/MM calculations, the ground-state singlet and the lowest triplet states were described using restricted and unrestricted Kohn−Sham (RKS and UKS) treatments, respectively. In addition, UKS calculations were performed for putative open-shell singlet species to check whether they may yield an open-shell (radical-type) configuration with energy lower than that of the closed-shell configuration. The residues included in the QM parts were truncated at appropriate sp^3-hybridized carbon atoms whenever possible. To be specific, FAD was represented by a lumiflavin comprised of the isoalloxazine ring, with a cut at the C1′−N10 bond (thus excluding the side chain), whereas Cys308 was truncated at the backbone. Lysine (K341, when included) was truncated at its C_β−C_γ bond (without the backbone part).

RESULTS AND DISCUSSION

Changes in the Active Site upon Substrate Binding. Theoretical acid dissociation constants (pK_a) were computed with PROPKA.[41] The resulting values are compiled for important active-site residues and NMT in Table 1. The pK_a analysis suggests that, at the optimum working conditions of MTOX (pH 8.0),[1] the stepwise addition of subunits (FAD and NMT) does not cause any change in the protonation states of key active-site residues. In contrast, isolated NMT is predicted to be in its zwitterionic form like other amino acids, whereas it is most likely ionized and assumes the anionic form in the binding pocket, as also indicated by the experimental pH profiles of MTOX with sarcosine as substrate.[7]

Judging from the computed pK_a values, the potential candidates as an active-site base that may receive a proton from the substrate amine prior to oxidation are the neutral lysines (K218, K259, K341) and the conserved H^+ exchanger (His263, protonated at the N_E position). In view of their close proximity to the backbone of the substrate NMT,[2] His263 and

DOI: 10.1021/cs501694q
ACS Catal. 2015, 5, 1227−1239

Table 1. Computed pK_a Values at Selected NMT Atoms and MTOX Residues in Different Model Systems: Isolated NMT and MTOX as well as MTOX-FAD and MTOX-FAD-NMT Complexes

atom/residue ID	only NMT	only MTOX[a]	MTOX-FAD[a]	MTOX-FAD-NMT[a]
NMT-N_{ter}	10.0			4.5
NMT-C_{ter}	5.0			−1.9
NMT-N_{ar}	4.5			2.6
Arg48		11.3	10.3	10.3
Arg51		11.4	11.3	13.1
Lys218		8.0	7.8	7.6
Tyr249		13.1	14.0	14.1
Lys259		5.9	5.8	5.7
His263		3.1	2.5	0.3
Lys341		6.2	5.6	7.7

[a]With a single crystal water molecule (see Computational Methodology).

K341 seem most suitable for this role. K259 is part of the Lys-H_2O-N5 motif conserved across amine oxidases and has already been shown to be the site of oxygen activation in MTOX.[6] The homologue of His263 in MSOX (H269) apparently does not act as an active-site base, since the turnover rate is only twice as slow as that in the H269N mutant.[10] Given the high structural homology between MSOX and MTOX,[3] one would not expect His263 to be the active-site base in MTOX either; however, this still needs to be proven. Unlike His263, which is essentially deprotonated before and after substrate binding (pK_a values of 2.5 and 0.3; Table 1), an equilibrium of the protonated and unprotonated forms is predicted for K341 (pK_a values of 5.6 and 7.7) that is slightly shifted toward the unprotonated form after substrate binding.

In contrast, the other previously nominated candidate, Tyr249, remains protonated/neutral in all cases (see Table 1), disabling it from taking up protons and acting as a base. This suggests that Tyr249 mainly has a steric role in substrate binding, which is consistent with the fact that mutation of its homologue in MSOX (Tyr317) only leads to a 20-fold decrease in the maximum rate of the reductive half-reaction.[9]

Dynamics of Substrate Binding. To cover all possible binding scenarios, we simulated 12 different NVT ensembles, which arise from combining the two conceivable protonation states of K259 and K341 with the three forms of the substrate NMT, while keeping K218 and His263 always unprotonated/neutral. We also investigated the K341Q mutant, with two protonation states of K259, to further analyze the role of K341. Some characteristic features extracted from each ensemble are compiled in Table S1 in the Supporting Information for direct comparison. The pK_a analysis does not give a clear preference between the nonzwitterionic or zwitterionic forms of neutral NMT (before ionization) in the active site. In the following, we thus consider both possible binding scenarios for neutral NMT on the basis of the NVT ensembles of wild-type MTOX.

In the case of zwitterionic NMT, the binding mode of the substrate is mainly determined by the protonation state of K341 (see Table S1 in the Supporting Information). If K341 is deprotonated, NMT remains rather far away in an unreactive position (R(Cs−N5) = 5.5−7.5 Å). NMT-NH_2 is in H-bonding distance with Gln247 (via O_E) and also in close contact (a) with the COO^- terminus and K341 (via bulk water) for deprotonated K259 or (b) with His263 for protonated K259. On the other hand, if K341 is protonated, the two subunits, FAD and NMT, are packed more closely (R(Cs−N5) = 3.4−4.2 Å), which is mainly due to the enhanced H-bond donor character of K341. In this case, NMT-NH_2 is engaged in a H-

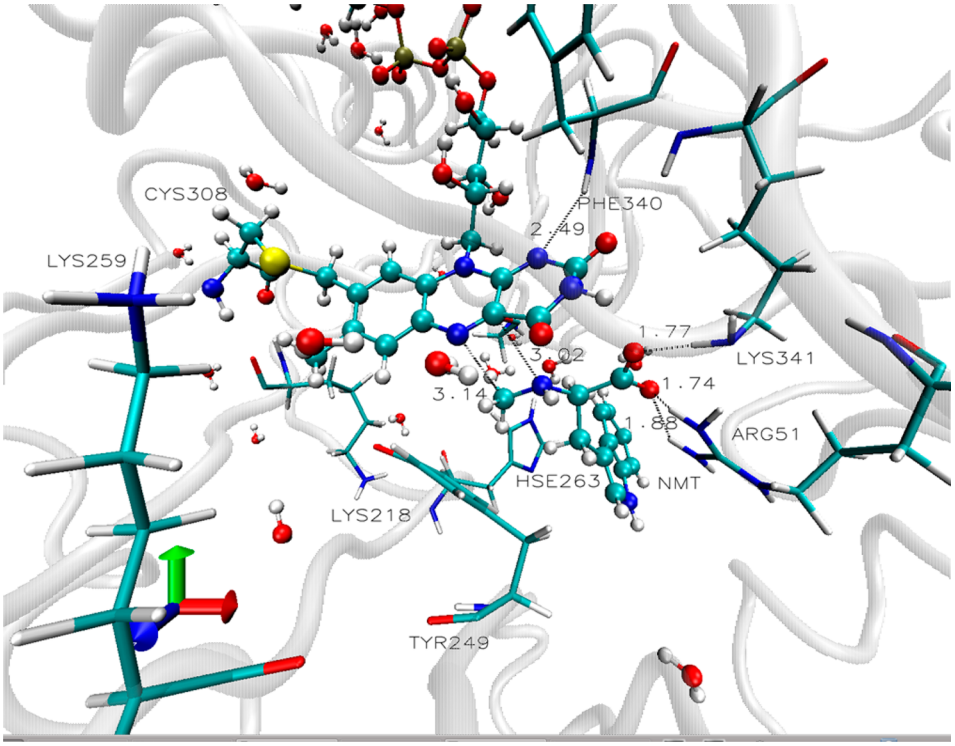

Figure 3. Typical snapshot from the NVT ensemble for AnNMT (K259, protonated; K341, deprotonated). Depicted are FAD and NMT (ball and stick), important MTOX residues (stick), and the MTOX structure (cartoon).

DOI: 10.1021/cs501694q
ACS Catal. 2015, 5, 1227−1239

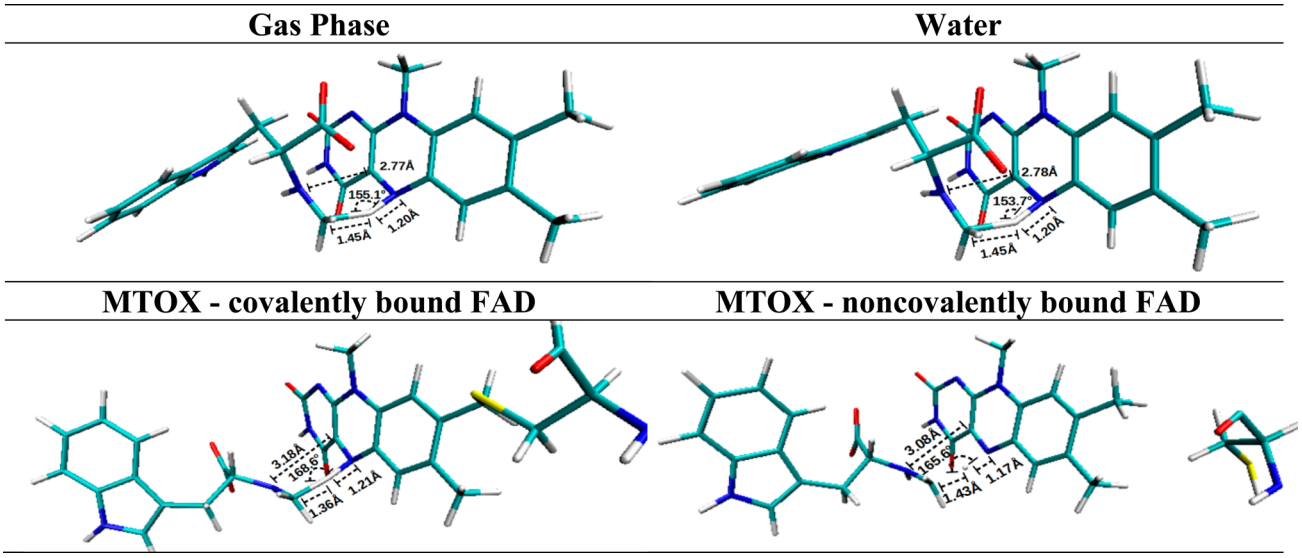

Figure 4. Geometries of the transition state for the HT pathway (^{1}**TS**) in different environments: (top) QM(B3LYP-D2/6-31G(d)) structures; (bottom) QM/MM structures (QM region only). Key structural parameters are included; more data are given in Tables S6 and S7 in the Supporting Information. See Figure 1 for labels and the text for the model system definitions.

bonding network with Gly337 (via backbone-O), His263, and bulk water.

Nonzwitterionic NMT is found to exhibit proper and stable binding only when K259 is protonated (see Table S1 in the Supporting Information). In this case, the N-terminus of NMT has no H-bonding partner, and K341 is the main H-bonding partner of the C terminus in line with its designated role as active-site base. The protonation state of K341 determines the other partner in the H-bonding network (Arg51-Tyr54 or Leu49) as well as the compactness of the reactive centers on FAD and NMT, with unprotonated K341 providing a more compact binding (Table S1).

The H-bonding networks encountered in different NVT trajectories suggest that the extra proton on the N-terminus of ZwNMT can be delivered to (a) the nearby bases (His263 and K341), (b) the N1 atom on FAD via Gly337, or (c) the C terminus of NMT (with conversion to the nonzwitterionic form). In contrast, the extra proton on the C terminus of Non-ZwNMT can be delivered easily to K341, which is always located in H-bonding distance of Non-ZwNMT. The NVT ensembles show the formation of a proton relay system involving Tyr54, His338, and K341 (see Figure S1 in the Supporting Information), while His263 has direct access to bulk water in each of the NVT ensembles. Hence, both K341 and His263 are suitable to act as a base.

On the other hand, the putative proton relay system proposed for MSOX[9,11] via a proton shuttle to N5 or K259 (direct or via water molecules) seems unlikely in MTOX. This is because such a proton shuttle is not seen in any of the NVT ensembles with a neutral NMT form, except for the special case of Non-ZwNMT with both K259 and K341 being unprotonated. In this latter case, a direct H bond between N5 and COOH of NMT is formed for very short periods, making this interaction fleeting and unreliable. However, a direct proton shuttle (via water molecules and without including N5) between the N terminus of NMT and K259 is not found in any of these NVT trajectories, as opposed to the case of its homologue (K661) in LSD1.[33] Taken together, these findings are congruent to the proposed role of K259 in oxygen activation rather than in amine oxidation, as deduced from experimental mutation studies.[6]

A stable binding of AnNMT, the anticipated reactive form, is achieved only in one case: when K259 is protonated and K341 is unprotonated (see Figure 3). In the corresponding MD trajectory, two conditions are satisfied that were previously shown[33,34] to be required to facilitate the transfer of a hydride equivalent, namely the close proximity of the reactive centers (N5 and Cs, average distance 3.37 Å) and a nonbonded Ns−C4a interaction (average distance 3.09 Å) involving the Ns lone pair and the π^* orbital (C4a−N5). The H-bond donors (K341, R51, and Y54) appear to be important for the close packing of the two subunits. Moreover, this MD trajectory sustains the N5-H_2O-Lys motif that is conserved across amine oxidase families,[6] with an expansion of the standard motif by an extra water molecule.

The microenvironment in MTOX has a delicate electrostatic balance, and hence changes in the active site may result in partial or complete failure of AnNMT binding. To quote a specific example, when K218 is protonated, we could not obtain a proper reactive binding of the substrate (i.e., R(N5−Cs) > 6.0 Å) for any combination of the K259 and K341 protonation states. On the other hand, if His263 were fully protonated (on both N_D and N_E) in contrast to the pK_a analysis (*vide supra*), there would be a loose yet reactive binding of the substrate (R(N5−Cs) = ca. 3.59 Å). The trajectory for the H263N mutant, in contrast, features three different arrangements, with R(N5−Cs) distances of ca. 4.1, 5.6, and 7.0 Å, respectively (see Figure S2 in the Supporting Information), which suggests that any reactive binding in the H263N mutant (R(N5−Cs) = ca. 4.1 Å) is clearly not as persistent as in the wild type (see Figure S2). This supports the role of His263 (His269 in MSOX) of aligning the substrate in a reactive position via π-stacking interactions.

The K341Q mutant appears to bind the substrate in a reactive orientation (albeit somewhat looser, R(N5−Cs) = ca. 3.31 Å; Figure S2 in the Supporting Information). The H-bonding partners of the NMT/C terminus differ slightly in the mutant and the wild type: R51 and K341/Q341 are common to

DOI: 10.1021/cs501694q
ACS Catal. 2015, 5, 1227−1239

Table 2. QM-Only Gibbs Free Relative Energies (in kcal/mol) of the Stationary Points (Figure 1) for Three Different Forms of NMT, Computed at the B3LYP-D2/6-31G(d) Level in the Gas Phase and Water[a]

	HT pathway (singlet manifold)			SET pathway (singlet manifold)			SET pathway (triplet manifold)		
NMT type	^{1}RC	^{1}TS	^{1}PC[b]	^{3}RC	^{3}TS	^{3}PC	^{3}RC	^{3}TS	^{3}PC
				Gas Phase					
nonzwitterionic	0.0	41.3 (435*i*)	22.1	*c*	41.0 (784*i*)	*c*	54.0	60.7 (335*i*)	37.5
zwitterionic[d]	0.0								
anionic	0.0	31.0 (1102*i*)	19.1	*c*	*c*	*c*	25.1	36.3 (1090*i*)	36.2
				Water					
nonzwitterionic	0.0	40.7 (693*i*)	18.7	*c*	*c*	*c*	46.9	52.2 (141*i*)	39.0
zwitterionic	0.00	58.3 (771*i*)	23.9	*c*	54.0 (918*i*)	48.8	34.6	60.0 (1995*i*)	46.9
anionic	0.0	26.5 (1160*i*)	14.7	*c*	*c*	*c*	29.2	31.7 (924*i*)	29.2

[a]The complete list of results for the different density functionals and basis sets can be found in Table S4 in the Supporting Information. [b]An adduct with a Cs−N5 covalent bond is formed for the nonzwitterionic and zwitterionic forms of NMT, but not for the anionic form. [c]Yields the closed-shell configuration. [d]Yields the nonzwitterionic form.

both, whereas Tyr54 in wild-type MTOX is replaced with FAD-N3 in K341Q. The latter replacement is likely the main reason for the slightly increased separation between the two reactive centers. These findings suggest that K341 is not vital for the proper orientation of the COO^- end of AnNMT, as another neutral amino acid could provide the required steric effects as well.

Reductive Activity of Different NMT Forms. We performed QM-only (gas phase and water) and QM/MM (protein environment) calculations to locate the stationary points of the three proposed amine oxidation pathways (PN, HT, and SET; Figure 1). During these calculations, we separately considered the three forms (nonzwitterionic, zwitterionic, and anionic) of the NMT substrate. For sampling purposes, we used several snapshots from different NVT ensembles of each NMT form as the starting geometries for QM/MM calculations. As discussed earlier, a reactive binding of NMT (i.e., with low Cs−N5 distance) can be achieved only for specific combination(s) of the protonation states of K259 and K341 for each NMT form (see Table S1 in the Supporting Information). The combinations used in the corresponding NVT ensembles are documented in Tables S2 and S3 in the Supporting Information, along with some key features of these NVT ensembles. Despite serious attempts, we could not locate the adducts A and B (PN pathway, Figure 1) as stable minima, neither in QM-only nor in QM/MM calculations. This is likely due to van der Waals repulsions caused by the bulky methyl group flanking the Ns atom in NMT, which will then prevent the formation of a covalent Ns−C4a bond. Therefore, from now on, we will only consider the two feasible pathways (HT and SET).

The QM-only calculations were done on a model system, which contains the isoalloxazine moiety of FAD (taken as lumiflavin, including the methyl group bound to N10) and one of the three forms of the substrate NMT (with a total of 60−61 atoms depending on the NMT form considered; see Figure 4, top panel). Benchmark calculations using four density functionals (performed in the gas phase and water with Non-ZwNMT; Table S4 in the Supporting Information) indicate that the Gibbs relative free energies from different functionals may differ noticeably, but the trends in these energies do not depend on the choice of the functional. Likewise, the use of a larger basis, TZVP, has only a small effect on the predicted Gibbs relative free energies (0.1−5 kcal/mol, see Table S4: B3LYP and B3LYP-D2, Non-ZwNMT in the gas phase) and, more importantly, does not alter the qualitative picture. Comparison of the energetics from B3LYP and B3LYP-D2 (Table S4) demonstrates that accounting for dispersion corrections has a more significant effect on the predicted activation barriers (raised or lowered by 2−10 kcal/mol) for the HT and SET mechanisms of all NMT forms. This is not surprising, since the model system consists of two aromatic subunits with a high degree of π stacking that leads to strong dispersion interactions. Previous QM/MM studies have shown that the inclusion of dispersion effects can significantly improve the accuracy of calculated barriers for enzymatic reactions[53,54] and that B3LYP/MM calculations without dispersion corrections may yield qualitatively wrong reaction energetics.[55] Given this situation, we will focus on the B3LYP-D2/6-31G(d)-based results in the remainder of this article. The corresponding free energies are documented in Table 2 for all three NMT forms in the gas phase and in water.

It is evident from the activation barriers for both the HT and SET pathways in the gas phase and in water that the anionic form of NMT is more reactive than the two neutral forms (Table 2). In water, the preference for the anionic form is more clear-cut than in the gas phase, probably because of the enhanced stabilization of the CT-complex species by the polar environment. For analogous reasons, the activation barriers on the HT and SET pathways are further reduced for anionic NMT in water by about 5 kcal/mol. Interestingly, in both the singlet and triplet manifold, the SET pathway is more favored for the neutral NMT forms than for anionic NMT, which prefers the HT pathway. The associated barriers, however, are close to each other in energy, thus preventing a conclusive verdict. In addition, other density functionals (except M06-2X) also predict a TS species on the broken-symmetry singlet SET pathway corresponding to a singlet-coupled radical pair of nonzwitterionic NMT and FAD, in the gas phase and in water (Table S4 in the Supporting Information).

In the gas phase, the zwitterionic form of NMT is not stable and spontaneously converts back to the nonzwitterionic form, whereas the two charged centers are properly stabilized in water. However, the transfer of a hydride equivalent is significantly less facile in the zwitterionic than in the nonzwitterionic form. The reactant complex (^{1}**RC**) with the zwitterionic form is only about 0.5−2.3 kcal/mol less stable than that with the nonzwitterionic form; thus, the strong decrease of the amine oxidation rate in water can be ascribed to the high destabilization of the TS species. The low energy difference of the two forms in water also points to a high rate of the interconversion between them.

DOI: 10.1021/cs501694q
ACS Catal. 2015, 5, 1227−1239

Table 3. QM(B3LYP-D2/6-31G(d))/MM Relative Energies (Gibbs Relative Free Energies in Parentheses) for the Stationary Points (Figure 1) of the HT and SET Mechanisms for Different NMT Forms with Noncovalently or Covalently Bound FAD: Average Values and Standard Deviations (kcal/mol) over a Set of Five Snapshots[a]

	HT pathway (singlet manifold)			SET pathway (triplet manifold)		
NMT type	^{1}RC	^{1}TS	^{1}PC	^{3}RC	^{3}TS	^{3}PC
			Covalently Bound FAD			
nonzwitterionic	0.00	41.3 ± 2.54	18.5 ± 4.14	44.2 ± 0.77	55.8 ± 2.24	36.0 ± 1.15
	(0.00)	(38.8 ± 2.57)	(20.8 ± 4.24)	(41.7 ± 0.82)	(51.0 ± 2.15)	(34.0 ± 1.36)
zwitterionic	0.00	65.6 ± 2.11	37.7 ± 3.65	39.2 ± 4.66	75.5 ± 1.03	46.7 ± 3.12
	(0.00)	(63.3 ± 2.32)	(39.2 ± 3.84)	(37.5 ± 4.41)	(72.4 ± 2.15)	(43.4 ± 3.10)
anionic (wild type)	0.00	24.1 ± 2.46	2.78 ± 2.11	27.7 ± 4.56	37.9 ± 2.80	30.8 ± 4.57
	(0.00)	(21.3 ± 2.27)	(5.04 ± 1.89)	(26.0 ± 4.00)	(34.1 ± 2.82)	(29.3 ± 4.66)
anionic (K341Q)	0.00	30.7 ± 0.30	15.1 ± 2.98	26.0 ± 3.12	43.5 ± 1.99	39.2 ± 2.78
	(0.00)	(28.4 ± 0.33)	(16.0 ± 2.70)	(24.2 ± 3.10)	(40.0 ± 2.09)	(37.8 ± 2.84)
anionic (H263N)	0.00	36.4 ± 5.73	5.56 ± 8.84	21.4 ± 6.12	49.1 ± 6.43	34.1 ± 4.31
	(0.00)	(33.5 ± 5.51)	(5.42 ± 8.10)	(19.3 ± 6.41)	(45.1 ± 6.09)	(32.2 ± 3.67)
			Noncovalently Bound FAD			
nonzwitterionic	0.00	34.8 ± 2.41	6.06 ± 1.85	38.4 ± 2.47	46.3 ± 4.9	28.3 ± 6.98
	(0.00)	(32.9 ± 2.50)	(9.40 ± 1.81)	(35.9 ± 2.73)	(45.4 ± 3.6)	(26.5 ± 6.9)
anionic	0.00	25.9 ± 3.09	2.71 ± 1.28	25.7 ± 2.74	36.2 ± 2.95	26.7 ± 2.59
	(0.00)	(23.3 ± 3.32)	(5.56 ± 1.46)	(23.5 ± 2.58)	(32.0 ± 2.92)	(24.5 ± 2.72)

[a]Results for the K341Q and H263N mutants are also given.

The amine oxidation process is likely affected by the immediate protein surrounding. Acting as a bridge between MTOX and FAD, Cys308 is expected to have a strong influence. Therefore, in order to capture the potential effects of the covalent binding of FAD on the reaction, the QM region was expanded in QM/MM calculations by inclusion of Cys308 (71−72 QM atoms; see Figure 4, bottom-left inset). The resulting B3LYP-D2/MM relative energies and free energies for the HT and SET pathways are compiled in Table 3 for different NMT forms as well as for different binding modes (non-covalent or covalent) of the cofactor FAD. Table 3 also contains the QM/MM results for the K341Q and H263N mutants. Evidently, AnNMT is the most reactive form on both the HT and SET pathways in line with expectations, and we will thus focus on AnMNT in our further comparisons. All available energy values associated with AnNMT are visualized in Figure 5, and the corresponding QM-only and QM/MM geometries with AnNMT are shown in Figure S3 in the Supporting Information.

To check the effect of basis set extension on QM/MM energetics, we evaluated for a single snapshot (with AnNMT) the single-point QM(B3LYP-D2/TZVP)/MM relative energies at the QM(B3LYP-D2/6-31G(d))/MM geometries. Likewise, we also checked the effect of expanding the QM region by including all of the active-site residues that are in close contact (within 5 Å) with the substrate NMT: viz., L49, I50, R51, Y54, G55, E56, T239, Q247, Y248, Y249, H263, E316, H338, and K341 (for a total of 299 QM atoms, visualized in Figure S4 in the Supporting Information). The single-point QM(B3LYP-D2/6-31G(d))/MM relative energies were computed using the expanded QM region at the geometries available from the standard QM region. For a direct comparison, all the computed energies are compiled in Table S5 in the Supporting Information. Inspection of Table S5 shows that extension of the basis set slightly lowers the computed relative energies (minor changes up to 3 kcal/mol). The effect of expanding the QM region is somewhat more pronounced (changes of 1−5 kcal/mol, with a trend to alleviate the activation barriers for the HT and SET mechanisms), which is likely due to the improved treatment of nonbonded interactions. However, in both cases, the overall qualitative picture does not change. Therefore, and also considering the computational efforts involved, we will primarily discuss the QM/MM results obtained with the standard QM region and 6-31G(d) basis in the following (unless explicitly stated otherwise).

For the amine oxidation in the MTOX environment, the anionic form of NMT is preferred over the neutral forms (Table 3), as in the gas phase and in water (Table 2). Likewise, the zwitterionic form again yields the lowest oxidation rates, regardless of which pathway is considered (HT or SET). Different levels of reactivity of the different NMT forms may be attributed to the degree of compactness of the resulting FAD-NMT complex. As is evident from Table S2, AnNMT provides the most compact reactive core in the reactant complex, with a smaller separation between the reactive centers (R(N5−Cs) = 3.09 ± 0.13 Å). AnNMT also provides an enhanced nonbonded Ns−C4a interaction (R(Ns−C4a) = 3.37 ± 0.17 Å). On the other hand, ZwNMT leads to a looser binding of the two subunits, mainly due to H bonding of the N terminus of NMT to Gly337 (unlike the Non-ZwNMT and AnNMT forms). This keeps Ns rather far away from the N5−C4a locus of FAD and greatly weakens the Ns−C4a interaction (4.25 ± 0.31 Å). In contrast, the N5−Cs distance takes an intermediate value (3.51 ± 0.20 Å) between those for Non-ZwNMT and AnNMT (4.07 ± 0.26 and 3.37 ± 0.17 Å), whereas the alignment of C4a−N5 and Ns−Cs bonds differs significantly in ZwNMT and in the two other forms (θ(Ns−Cs−N5−C4a) = −3° vs 48°). We note that the alignment of the C4a−N5 and Ns−Cs bonds is highly important, as it affects the strength of the nonbonded C4a−Ns interaction.

Mechanistic Insights into the HT and SET Pathways. The HT mechanism involves the transfer of one proton and two electrons from NMT to FAD in a single concerted step (as hydride anion). We make use of a closed-shell description at the restricted Kohn−Sham (RKS) level for this process that converts the reactant complex ^{1}**RC** via the transition state ^{1}**TS** to the product complex ^{1}**PC**. The radical-SET mechanism, in contrast, proceeds through open-shell intermediates (Figure 1).

DOI: 10.1021/cs501694q
ACS Catal. 2015, 5, 1227−1239

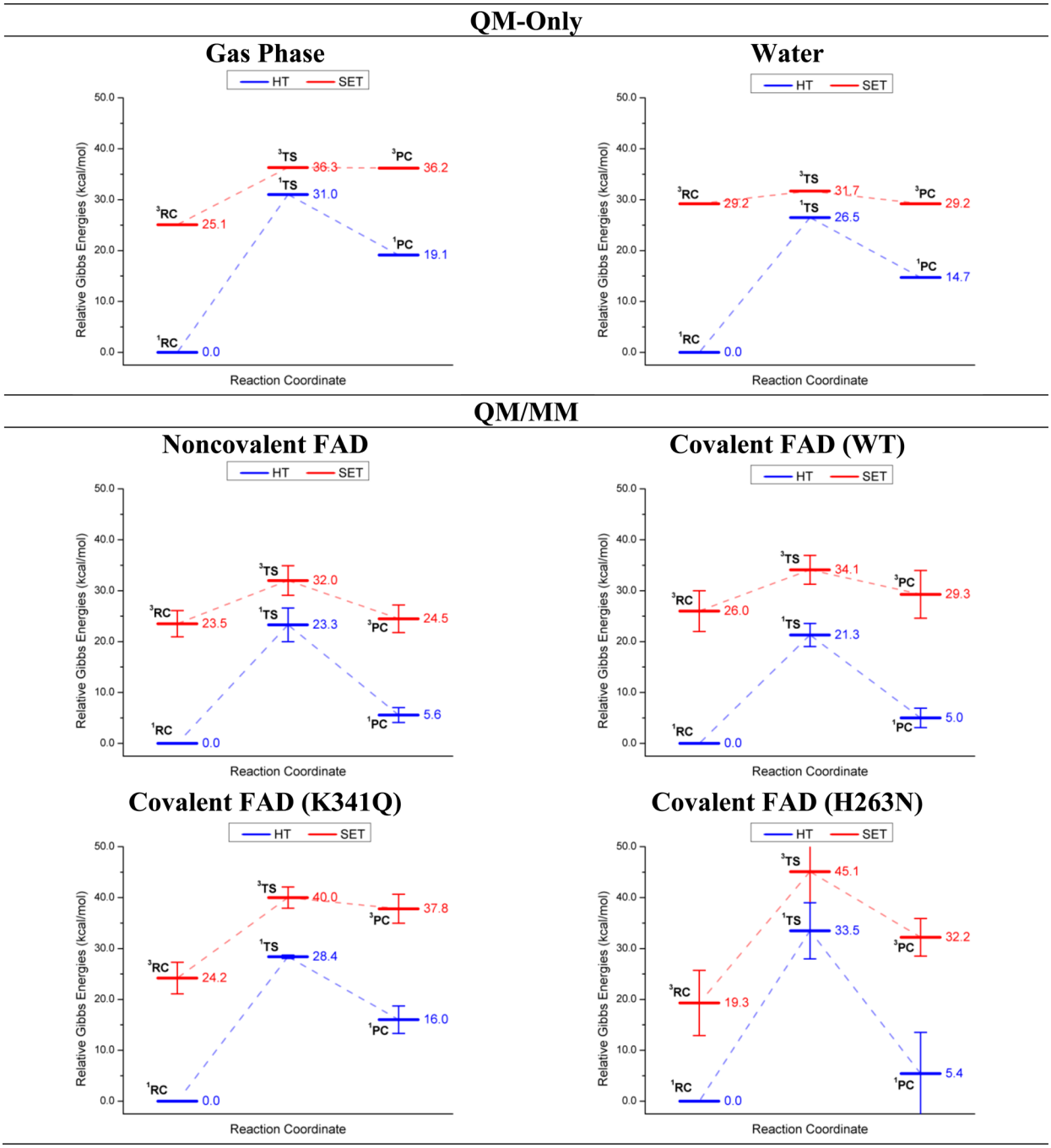

Figure 5. QM(B3LYP-D2/6-31G(d))-only and QM/MM Gibbs free energy profiles (in kcal/mol) of AnNMT for HT and SET pathways in different media and in MTOX with different model systems (see text for definitions). See Figure 1 for the definition of the stationary points.

The single-electron transfer from the α-C−H bond of NMT to FAD generates two radical intermediates (^{3}**RC**): namely the flavin semiquinone anion (**FAD**$^{\bullet-}$) and amine radical cation (**NMT**$^{\bullet+}$). The subsequent rate-limiting step is the homolytic cleavage of the α-C−H bond, which leads to the iminium cation (^{1}**PC**). The latter may undergo different reactions: (a) proton-coupled electron transfer (PCET) or direct hydrogen atom transfer and (b) stepwise transfer of a proton and an electron (second SET) from the amine to FAD. In the latter case, the initial proton transfer yields an intermediate pair of ammonium and FADH$^{\bullet-}$ radicals (^{3}**PC**), and the second SET step can occur directly or may also be mediated by adduct formation in the presence of an active-site radical.[16,18] The open-shell species on the SET pathways were described by the unrestricted Kohn−Sham (UKS) method. As the two unpaired electrons on the two separate subunits of the model system can have the same or different spin, we considered both the singlet and triplet manifolds. In contrast to the QM-only case (gas phase and water; Table 2), the broken-symmetry UKS calculations always converged to the closed-shell solution at the QM/MM level for any of the NMT substrate forms (as is evident from the computed energies, $\langle S^2 \rangle$ values, and spin densities; data not shown). The same was found when using restricted open-shell Kohn−Sham (ROKS) calculations for the QM region. Therefore, only triplet SET values are included in Table 3 and Figure 5.

DOI: 10.1021/cs501694q
ACS Catal. 2015, 5, 1227−1239

Hybrid QM/MM calculations on MTOX with a covalently bound FAD and the most reactive NMT form (AnNMT; see Figure 5) predict a free energy barrier of 21.3 ± 2.3 kcal/mol for the HT mechanism (approximate rate 0.087 min^{-1}), whereas the QM-only calculations yield barriers of 31.0 kcal/mol in vacuum and 26.5 kcal/mol in water. The protein environment thus increases the HT rate dramatically in comparison to water (by 4 orders of magnitude). In contrast, the MTOX environment increases the corresponding activation barrier for the SET mechanism in comparison to the polar solvent (34.1 ± 2.8 vs 31.7 kcal/mol), thus lowering the SET rate by 2 orders of magnitude. The computed SET rate in MTOX is approximately 3.5×10^{-11} min^{-1}, rendering the HT pathway clearly favorable at physiological temperatures.

To probe the possible reasons why the most reactive AnNMT form prefers the HT pathway in all media, we compiled key structural features in the QM-only and QM/MM geometries (averages over five snapshots) of the stationary points for the two pathways in Tables S6 and S7 in the Supporting Information. For the HT pathway, we note a gradual increase in the compactness of the reacting subunits in the reactant complexes (^{1}**RC**), as is evident from the Cs−N5 distances (gas phase, 3.82 Å; water, 3.33 Å; MTOX, 3.01 Å). Thus, the increase in the HT rates on going from the gas phase to the protein environment can be linked to the enhanced interaction of the reactive sites (N5 and Cs). This is reminiscent of the increase in the computed HT rates when going from neutral to anionic NMT that can also be attributed to the tighter binding in the latter case (see Reductive Activity of Different NMT Forms).

Likewise, the environment mainly affects the separation of two reacting centers in the product complex (^{1}**PC**). The ^{1}**PC** species is a weakly interacting complex in the gas phase and in water (R(Cs−N5) = 2.08 and 2.06 Å, respectively) but forms an adduct in the protein environment (1.69 Å). This has evident consequences for the energetics (Figure 5): the ^{1}**PC** adduct is more stable than the weakly interacting ^{1}**PC** species (relative free energies: 5.0 ± 1.9 vs 14.7 kcal/mol), even though the reaction remains endergonic. The ^{1}**PC** adduct contains a covalent bond between the α-carbon atom of the amine substrate and the N5 atom of FAD, as also found for other amine oxidases.[32,33]

In the mechanism of amine demethylation,[12] the initial amine oxidation is followed by the hydrolysis of the formed iminium cation. To prepare for this second step, the covalent bond in the FAD−imine adduct (^{1}**PC**) needs to be broken to yield a weakly interacting complex with a separate iminium cation. In the case of MAO-B, a two-step mechanism has been proposed for the dissociation of the initial adduct,[32] which involves the transfer of a proton from the flanking nitrogen in the (protonated) substrate (here called Ns) via two active-site water molecules located on the *Re* face of FAD. This proton transfer was suggested to facilitate the breaking of the covalent N5−Cs bond, which generates the final product complex between the reduced flavin FADH anion and the iminium cation. In the case of MTOX, active-site water molecules are not present in any NVT ensemble with any NMT form (see Table S2 in the Supporting Information), which makes the proposed two-step mechanism questionable. However, instead of water, the Gly337, Phe340, and K341 residues (all in H-bonding distance to N1 and O2) might serve as potential mediators for the proton transfer to the N1 atom of FAD.

To investigate the feasibility of a hydride equivalent transfer in the case of FAD protonated at N1, we generated the corresponding starting structures from either one of two neutral NMT forms (ZwNMT or Non-ZwNMT) by manually shifting the proton from NMT-Ns or NMT-COOH, respectively, and then computing reaction profiles for the HT pathway. In the case of ZwNMT, the resulting energetics at optimized geometries (Table S8) show that the overall barrier is indeed reduced by ca. 8 kcal/mol after N1 protonation, but it is still very high (55.7 kcal/mol). In addition, the intermediate ^{1}**RC** species with a FAD protonated at N1 is much less stable (by 45.7 kcal/mol) in comparison to that with unprotonated N1. In the case of Non-ZwNMT, this ^{1}**RC** species (with protonated N1) is destabilized less (by 18.0 kcal/mol, relative to the ^{1}**RC** species with unprotonated N1); we have not computed the barrier to its formation by proton transfer to N1. Given the overall low energy required for the favored HT pathway with AnNMT and unprotonated FAD-N1 (22.1 kcal/mol), a mechanism involving N1 protonation prior to HT seems quite improbable. Furthermore, N1 protonation after HT would require a neutral form of the substrate to react, which can be excluded because the anionic form is much more reactive (see Reductive Activity of Different NMT Forms). On the basis of these findings, we propose that the formed ^{1}**PC** adduct will react spontaneously: (a) by reprotonation of the backbone of the imine product to convert it back to neutral NMT, (b) by protonation of the N1 atom of FAD after the hydride transfer, or (c) as part of a larger collective protein movement, such as the release of the substrate out of the active site (on a longer time scale).

In contrast to the situation in the ^{1}**RC** and ^{1}**PC** species, the MTOX environment does not have a significant effect on the distance between the reactive centers in ^{1}**TS** (R(Cs−N5) = 2.55−2.58 Å). However, it notably affects the hydride transfer angle (θ(Cs−H1−N5)) and the alignment of the C4a−N5 and Cs−Ns bonds (θ(Ns−Cs−N5−C4a)) (see Tables S6 and S7 in the Supporting Information and Figure 4). The active-site residues in MTOX enforce a more linear path for the hydride transfer in comparison to the gas phase and water (θ(Cs−H1−N5) = 169° vs 154−155°), We note in this connection that MTOX also employs an HT arrangement more linear than that of LSD1[33] and MAO-B[34] (θ(Cs−H1−N5) = 150−155°).

On the radical-SET pathway, the first SET from NMT to FAD creates a radical pair (^{3}**RC**), which has already been shown to be energetically demanding in LSD1.[33] Although we did not compute the energy required for intersystem crossing ($S_0 \rightarrow T_1$, conversion of ^{1}**RC** to ^{3}**RC**), it is expected to be lower than the barrier of the rate-limiting homolytic cleavage of the α-C−H bond (i.e., ^{3}**TS** of the SET pathway).[13,26] The resulting radical pair is computed to be of high energy in the gas phase and water (25.1 and 29.2 kcal/mol, respectively). There is no significant stabilization by the MTOX environment (26.0 ± 4.0 kcal/mol), so that the radical pair remains an unfavorable intermediate prior to the homolytic cleavage of the α-C−H bond on the SET pathway. Given the rather low barrier for the subsequent proton transfer in MTOX (^{3}**RC** → ^{3}**TS**: 8.1 kcal/mol), the radical pair can be converted rather easily to radical products (^{3}**PC**) that are also unstable (29.3 ± 4.7 kcal/mol). However, this low proton transfer barrier is kinetically irrelevant, as the SET process is inaccessible due to the high overall barrier (^{3}**TS**: 34.1 ± 2.8 kcal/mol).

To check whether the active-site residues in MTOX may contribute to the stabilization of the radical pair (^{3}**RC**), we

DOI: 10.1021/cs501694q
ACS Catal. 2015, 5, 1227−1239

computed the QM/MM energies and spin densities with an extended QM region (vide supra). It is evident from the spin densities (Figure S5 in the Supporting Information) that a radical pair of FAD and NMT is formed as expected for the SET pathway, since none of the neighboring MTOX residues take up part of the unpaired electron density (neither in ^{3}**RC** nor in the other stationary points on the SET pathway). The QM/MM results with the extended QM region lower the relative energy of ^{3}**RC** only slightly (by ca. 4.0 kcal/mol; Table S5 in the Supporting Information), presumably due to the QM treatment of active-site H-bonding interactions.

Judging from the key structural parameters (Tables S6 and S7 in the Supporting Information), the protein environment makes the reactive core in the stationary points of the SET pathway more compact (as in the case of the HT pathway). On the other hand, a product adduct is not formed on the SET pathway (^{3}**PC**) in any medium, as opposed to the HT pathway (^{1}**PC**; see the Cs−N5 distances in Tables S6 and S7). Attempts to enforce a ^{3}**PC** adduct ended up with extremely unstable species (ca. 80 kcal/mol), which is as expected, since two subunits with unpaired electrons of the same spin will tend to stay apart rather than form an adduct.

Catalytic Role of His263 and Lys341. To further augment our understanding of the role of the two most likely active-site base candidates, we extended the QM/MM calculations for wild-type MTOX by including either H263 or K341 in the QM region (data not shown), and we also investigated the H263N and K341Q mutants (Table 3 and Figure 5). Including H263 or K341 in the QM part leads to only minor reductions of the HT and SET barriers (by 1 and 2−3 kcal/mol, respectively), and Mulliken population analysis shows almost no changes in the charge distribution in the reactive core (Cs, N5, Ns, and C4a) of ^{1}**RC**, ^{1}**TS**, and ^{1}**PC** (data not shown). However, inclusion of K341 in the QM part does affect the charges of the oxygen atoms at the C terminus, reflecting the electrostatic influence of K341. Furthermore, on the SET pathway, no spin density is found on these residues in ^{3}**RC**, ^{3}**TS**, and ^{3}**PC**. Taken together, all of these findings imply that His263 and Lys341 do not have a catalytic role in MTOX.

The computed QM/MM energies (Figure 5) indicate a substantial decrease in the HT and SET rates in both the H263N and K341Q mutants, in comparison to wild-type MTOX. As discussed earlier, the H263N mutation does not support a stable AnNMT binding, since R(N5−Cs) remains generally larger than 5 Å in MD simulations (Figure S2 in the Supporting Information). In contrast, the K341N mutation weakens the binding only slightly, with R(N5−Cs) increasing by 0.10−0.15 Å (Table S2 in the Supporting Information). Even though we deliberately chose snapshots for QM/MM from the H263N MD trajectory with the closest possible contact between two reactive sites, the resulting HT and SET barriers are much higher in H263N than in K341Q. In this regard, QM/MM calculations suggest that His263 is more important for substrate alignment in MTOX than in MSOX, in which the mutant of the H263 homologue (H269N) has only a 2-fold slower turnover rate.[10] This may be related to the different nature of the substrates for MTOX (*N*-methyltryptophan) and MSOX (sarcosine). In particular, sarcosine lacks the aromatic indole side chain that could provide π-stacking and π−cation interactions with His263 and Arg51, respectively. In contrast, the current QM/MM results indicate only a partial reduction of the HT rate in K341Q in comparison to wild-type MTOX. This is likely due to electrostatic (stabilization of COO^-) effects of K341 rather than to steric effects (substrate binding; see MD results in Dynamics of Substrate Binding). The current QM/MM results do not rule out an active-site base role for K341, but they also do not directly support this possibility.

Effects of FAD Covalent Binding on Substrate Binding and NMT Oxidation. It has been proposed that the covalent binding of the flavin cofactor in MSOX and similar oxidases enhances protein stability (by avoiding the loss of a weakly bound oxidized cofactor) and improves enzymatic activity (by increasing the flavin redox potential and aiding substrate binding).[4,5] To probe the molecular basis for the catalytic role of FAD covalent binding, we created an artificial model system, with FAD noncovalently bound to MTOX, and compared it to wild-type MTOX. Specifically, we capped the Cys308-S and FAD-8α-methyl ends with hydrogen atoms, while the rest of the system was kept intact (73−74 atoms in the QM part; see Figure 4 for visualization). We repeated our standard computational procedure using this model system and the three forms of the NMT substrate. We present key features of the resulting NVT trajectories in Table S3 in the Supporting Information, the computed QM/MM energies in Table 3 and Figure 5, and key structural properties in Table S7 in the Supporting Information.

We first note that there is no stable binding of AnNMT in any of the NVT trajectories with noncovalently bound FAD, whereas ZwNMT and Non-ZwNMT bind properly and even more compactly in comparison to their counterparts in the covalently bound FAD case (see R(Ns−C4a) and R(N5−Cs) values in Tables S2 and S3 in the Supporting Information). For further analysis, we inspected how the planarity of FAD is affected by its binding mode. To this end, we monitored six dihedral angles within the isoalloxazine moiety of FAD (θ(C9−C8−C7−C6), θ(C9−C9a−C5a−C6), θ(N10−C9a−C5a−N5), θ(N10−C10a−C4a−N5), θ(N1−C10a−C4a−C4), θ(N1−C2−N3−C4)) throughout the NVT trajectories of different NMT forms (Table S9 in the Supporting Information). Judging from the sum of the average absolute deviations from the reference values at planarity, the isoalloxazine moiety is closer to planarity in the case of noncovalent FAD binding (42−43° vs 61−68° for covalent FAD binding). It is (almost) perfectly planar in FAD without the protein environment (data not shown). These findings are in accord with previous arguments that the nonplanarity of FAD is the main factor in modulating the reduction potential of MSOX and other oxidases.[24] However, the current MD simulations do not provide evidence that MTOX enforces FAD to assume a "butterfly bent" structure, as proposed for TMADH.[56] This may be due to the differences in the binding sites of FAD in the two oxidases, which impose different constraints on the isoalloxazine moiety.

Since AnNMT does not bind properly in our artificial model system with noncovalently bound FAD, we assumed in our QM/MM calculations that the substrate binds in the Non-ZwNMT form, which is computed to afford the tightest binding (Table S3 in the Supporting Information) and that, being in close contact with unprotonated K341, NMT then donates its extra proton to the C terminus right before the transfer of the hydride equivalent. The QM/MM energies (Table 3 and Figure 5) indicate that the barrier for the HT pathway is slightly higher (by 2.0 kcal/mol) with noncovalently (rather than covalently) bound FAD. This increase is of the same magnitude as the previous estimate for the increase in reduction potential of

DOI: 10.1021/cs501694q
ACS Catal. 2015, 5, 1227−1239

MSOX due to covalent FAD binding (120 mV ≈ 2.8 kcal/mol, assuming a one-electron transfer, on the basis of binding affinities of Cys315 mutants).[4] In line with this minor change in the energetics, the key structural features in the optimized stationary points of the HT pathway show only slight variations (see, for instance, R(Cs−N5), R(Ns−C4a), θ(Cs−H1−N5), and θ(Ns−Cs−N5−C4a) in Table S7 in the Supporting Information).

CONCLUSIONS

Using results from theoretical pK_a analysis, classical MD simulations, and QM-only and QM/MM calculations, we present a comprehensive molecular-level analysis of the catalytic mechanism of the NMT oxidation catalyzed by MTOX, with special attention to the role of several active-site residues and covalent FAD binding. Our QM-only (gas phase and water) and QM/MM (protein environment) calculations predict that the anionic form (AnNMT) is far more reactive than the neutral forms of NMT, as expected in view of the optimum working conditions of MTOX (pH 8.0).[1] The QM-only and QM/MM results with AnNMT clearly favor the HT pathway over the radical/SET and adduct forming mechanisms, in accord with the previous computational studies on other flavoprotein oxidases.[26,32−34] In comparison to the protein-free environment (gas phase and water), MTOX expedites the HT rates markedly by lowering the activation barrier (21.3 ± 2.3 kcal/mol, corresponding to a rate of 0.087 min^{-1}), in reasonable agreement with the experimentally observed rates.[1,2] According to our computational results, the SET pathway requires the initial formation of a rather unstable radical pair (^{3}**RC**) and encounters an even higher activation barrier thereafter. The MTOX environment stabilizes neither the radical pair nor the transition state so that the SET pathway remains inaccessible in the enzyme. The adduct-forming (polar-nucleophilic) mechanism is ruled out on the grounds that the adducts formulated for this route (with an Ns−C4a bond; see Figure 1) are not stable intermediates and readily dissociate during QM-only and QM/MM optimizations.

On the HT pathway, the product species (^{1}**PC**) is computed to be an adduct of NMT-imine and FAD with a covalent Cs−N5 bond, congruent with the previous findings for other amine oxidases (MAO-B[32] and LSD1[33]). To break this adduct complex, a two-step HT mechanism was proposed in the case of MAO-B,[32] the second step of which involves protonation of the FAD at N1, with the proton coming from the N terminus of the amine substrate. Our MD simulations and QM/MM calculations do not support this mechanism in MTOX, for two reasons: (1) the mechanism requires that a neutral NMT species (ZwNMT or Non-ZwNMT) rather than AnNMT is oxidized, which is not feasible (computed barriers of 39 and 63 kcal/mol), and (2) the two water molecules needed to connect NMT-N and FAD-N1 to mediate the proton transfer are missing in MTOX. To check for an alternative variant of this mechanism, we presumed that Gly337 mediates the proton transfer, given its close proximity to the backbone of NMT and to FAD-N1 in the NVT ensembles. Hence, we checked the influence of an initial N1 protonation on NMT oxidation and found that, under these circumstances, oxidation may occur only for Non-ZwNMT, although it is much less facile than for the standard HT pathway with AnNMT. In view of these findings, we propose that the breakup of the adduct complex requires either reprotonation of the NMT backbone by the active-site base or protonation of FAD at N1.

Compliant with experimental studies on pH-dependent MTOX activity,[6,7] our computational findings indicate binding of neutral NMT in the active site, which is then ionized by an active-site base to give the reactive anionic form. Among the potential active-site bases proposed for MTOX (or MSOX that has high structural similarity[3]), we eliminate Tyr249 because of its location (MD simulations) and its protonation state (theoretical pK_a analysis), which is consistent with the only partial loss of activity upon mutation of its homologue in MSOX (Y317F).[9] MD simulations and QM/MM results suggest a steric role for His263 in orienting the substrate into the reactive position via π-stacking interactions; His263 appears to play a more eminent role in MTOX than in MSOX, considering the only 2-fold lower rates upon mutation of its homologue in MSOX,[10] which may be linked to the fact that MSOX genuinely works on a smaller aliphatic substrate. Our computational results indicate that K341 acts electrostatically and as an active-site base, which is consistent with the almost complete loss of MTOX activity (95% or 250-fold) upon K341Q mutation that is apparently not due to the 10% loss in FAD incorporation.[2]

MTOX employs FAD as the oxidizing agent, which is covalently bound to Cys308 via its C8 methyl group. Using an artificial theoretical model, with FAD noncovalently bound to MTOX, we scrutinized the role of the FAD binding mode. Our MD simulations show that a stable binding of anionic NMT is not likely in the case of noncovalent FAD binding. This is probably related to the more planar structures of the isoalloxazine ring that are seen in the MD simulations with noncovalent FAD. Flavin nonplanarity was proposed to be the reason for enhanced redox potentials of amine oxidases with a covalently bound flavin.[24,56] Our QM/MM results indicate a minor increase in the activation barriers for the HT pathway (by 2.0 kcal/mol) in the case of noncovalent binding.

ASSOCIATED CONTENT

Supporting Information

The following file is available free of charge on the ACS Publications website at DOI: 10.1021/cs501694q.

Computational details, characteristic features from NVT ensembles, complete set of QM-only results (gas phase and water) of three NMT forms with four density functionals, effect of extending basis sets and QM part on QM/MM energies, key structural properties from QM-only and QM/MM geometries, effect of protonating the FAD-N1 position on the HT and SET pathways, average deviation from planarity of the isoalloxazine ring in noncovalently and covalently bound FAD, proton relay system via K341, Cs−N5 distances in selected MD trajectories, and visualization of QM-only and QM/MM geometries, of the extended QM region, and of spin densities (PDF)

AUTHOR INFORMATION

Corresponding Author

*E-mail for W.T.: thiel@kofo.mpg.de.

Notes

The authors declare no competing financial interest.

ACKNOWLEDGMENTS

B.K. thanks Dr. Jan Götze, Dr. Mahendra Patil, and Dr. Mario Barbatti for valuable discussions in the course of this study.

DOI: 10.1021/cs501694q
ACS Catal. 2015, 5, 1227−1239

REFERENCES

(1) Khanna, P.; Schuman Jorns, M. *Biochemistry* **2001**, *40*, 1451−1459.
(2) Ilari, A.; Bonamore, A.; Franceschini, S.; Fiorillo, A.; Boffi, A.; Colotti, G. *Proteins* **2008**, *71*, 2065−2075.
(3) Koyama, Y.; Ohmori, H. *Gene* **1996**, *181*, 179−183.
(4) Hassan-Abdallah, A.; Zhao, G.; Jorns, M. S. *Biochemistry* **2006**, *45*, 9454−9462.
(5) Heuts, D. P. H. M.; Scrutton, N. S.; McIntire, W. S.; Fraaije, M. W. *FEBS J.* **2009**, *276*, 3405−3427.
(6) Bruckner, R. C.; Winans, J.; Jorns, M. S. *Biochemistry* **2011**, *50*, 4949−4962.
(7) Ralph, E. C.; Fitzpatrick, P. F. *Biochemistry* **2005**, *44*, 3074−3081.
(8) Wagner, M. A.; Trickey, P.; Chen, Z. W.; Mathews, F. S.; Jorns, M. S. *Biochemistry* **2000**, *39*, 8813−8824.
(9) Zhao, G.; Jorns, M. S. *Biochemistry* **2005**, *44*, 16866−16874.
(10) Zhao, G.; Song, H.; Chen, Z.-W.; Mathews, F. S.; Jorns, M. S. *Biochemistry* **2002**, *41*, 9751−9764.
(11) Zhao, G.; Jorns, M. *Biochemistry* **2006**, *45*, 5985−5992.
(12) Shi, Y.-J.; Lan, F.; Matson, C.; Mulligan, P.; Whetstine, J.; Cole, P.; Casero, R. A.; Shi, Y. *Cell* **2004**, *119*, 941−953.
(13) Gaweska, H.; Henderson Pozzi, M.; Schmidt, D. M. Z.; McCafferty, D. G.; Fitzpatrick, P. F. *Biochemistry* **2009**, *48*, 5440−5445.
(14) Forneris, F.; Binda, C.; Aglio, A. D.; Fraaije, M. W.; Battaglioli, E.; Mattevi, A.; Dall'Aglio, A. *J. Biol. Chem.* **2006**, *281*, 35289−35295.
(15) Khanna, P.; Jorns, M. *Biochemistry* **2001**, *40*, 1441−1450.
(16) Silverman, R. B. *Acc. Chem. Res.* **1995**, *28*, 335−342.
(17) Silverman, R. B. R.; Hoffman, S. S. J.; Catus, W. B. W. *J. Am. Chem. Soc.* **1980**, *102*, 7126−7128.
(18) Silverman, R. B. *Prog. Brain Res.* **1995**, *106*, 23−31.
(19) Miller, J. R.; Edmondson, D. E. *Biochemistry* **1999**, *38*, 13670−13683.
(20) Forneris, F.; Battaglioli, E.; Mattevi, A.; Binda, C. *FEBS J.* **2009**, *276*, 4304−4312.
(21) Culhane, J. C.; Cole, P. A. *Curr. Opin. Chem. Biol.* **2007**, *11*, 561−568.
(22) Fraaije, M. W.; Mattevi, A. *Trends Biochem. Sci.* **2000**, *25*, 126−132.
(23) Gaweska, H.; Fitzpatrick, P. F. *BioMol. Concepts* **2011**, *2*, 365−377.
(24) Scrutton, N. S. *Nat. Prod. Rep.* **2004**, *21*, 722−730.
(25) Fitzpatrick, P. F. *Arch. Biochem. Biophys.* **2010**, *493*, 13−25.
(26) Ralph, E. C.; Hirschi, J. S.; Anderson, M. A.; Cleland, W. W.; Singleton, D. A.; Fitzpatrick, P. F. *Biochemistry* **2007**, *46*, 7655−7664.
(27) Schmidt, D. M. Z.; McCafferty, D. G. *Biochemistry* **2007**, *46*, 4408−4416.
(28) Mccann, A. E.; Sampson, N. S. *J. Am. Chem. Soc.* **2000**, *122*, 35−39.
(29) Chen, Z. Z.; Zhao, G.; Martinovic, S.; Jorns, M. S.; Mathews, F. S. *Biochemistry* **2005**, *44*, 15444−15450.
(30) Wagner, M. A.; Jorns, M. S. *Biochemistry* **2000**, *39*, 8825−8829.
(31) Forneris, F.; Binda, C.; Vanoni, M. A.; Mattevi, A.; Battaglioli, E. *FEBS Lett.* **2005**, *579*, 2203−2207.
(32) Vianello, R.; Repič, M.; Mavri, J. *Eur. J. Org. Chem.* **2012**, *2012*, 7057−7065.
(33) Karasulu, B.; Patil, M.; Thiel, W. *J. Am. Chem. Soc.* **2013**, *135*, 13400−13413.
(34) Abad, E.; Zenn, R.; Kästner, J. *J. Phys. Chem. B* **2013**, *117*, 14238−14246.
(35) Trott, O.; Olson, A. J. *J. Comput. Chem.* **2010**, *31*, 455−461.
(36) Zhao, G.; Bruckner, R. C.; Jorns, M. S. *Biochemistry* **2008**, *47*, 9124−9135.
(37) Brooks, B.; Brooks, C. *J. ...* **2009**, *30*, 1545−1615.
(38) Luo, G.; Andricioaei, I.; Xie, X. S.; Karplus, M. *J. Phys. Chem. B* **2006**, *110*, 9363−9367.
(39) MacKerell, A. D.; Bashford, D.; Dunbrack, R. L.; Evanseck, J. D.; Field, M. J.; Fischer, S.; Gao, J.; Guo, H.; Ha, S.; Joseph-McCarthy, D.; Kuchnir, L.; Kuczera, K.; Lau, F. T. K.; Mattos, C.; Michnick, S.; Ngo, T.; Nguyen, D. T.; Prodhom, B.; Reiher, W. E.; Roux, B.; Schlenkrich, M.; Smith, J. C.; Stote, R.; Straub, J.; Watanabe, M.; Wiórkiewicz-Kuczera, J.; Yin, D.; Karplus, M. *J. Phys. Chem. B* **1998**, *102*, 3586−3616.
(40) Jorgensen, W. L.; Chandrasekhar, J.; Madura, J. D.; Impey, R. W.; Klein, M. L. *J. Chem. Phys.* **1983**, *79*, 926−935.
(41) Olsson, M.; Sondergaard, C.; Rostkowski, M.; Jensen, J. *J. Chem. Theory Comput.* **2011**, *7*, 525−537.
(42) Frisch, M. J.; Trucks, G. W.; Schlegel, H. B.; Scuseria, G. E.; Robb, M. A.; Cheeseman, J. R.; Scalmani, G.; Barone, V.; Mennucci, B.; Petersson, G. A.; Nakatsuji, H.; Caricato, M.; Li, X.; Hratchian, H. P.; Izmaylov, A. F.; Bloino, J.; Zheng, G.; Sonnenberg, J. L.; Hada, M.; Ehara, M.; Toyota, K.; Fukuda, R.; Hasegawa, J.; Ishida, M.; Nakajima, T.; Honda, Y.; Kitao, O.; Nakai, H.; Vreven, T.; Montgomery, J. A., Jr.; Peralta, J. E.; Ogliaro, F.; Bearpark, M.; Heyd, J. J.; Brothers, E.; Kudin, K. N.; Staroverov, V. N.; Kobayashi, R.; Normand, J.; Raghavachari, K.; Rendell, A.; Burant, J. C.; Iyengar, S. S.; Tomasi, J.; Cossi, M.; Rega, N.; Millam, J. M.; Klene, M.; Knox, J. E.; Cross, J. B.; Bakken, V.; Adamo, C.; Jaramillo, J.; Gomperts, R.; Stratmann, R. E.; Yazyev, O.; Austin, A. J.; Cammi, R.; Pomelli, C.; Ochterski, J. W.; Martin, R. L.; Morokuma, K.; Zakrzewski, V. G.; Voth, G. A.; Salvador, P.; Dannenberg, J. J.; Dapprich, S.; Daniels, A. D.; Farkas, O.; Foresman, J. B.; Ortiz, J. V.; Cioslowski, J.; Fox, D. J. *Gaussian 09, Revision D.01*, Gaussian Inc., Wallingford, CT, 2013.
(43) Becke, A. *J. Chem. Phys.* **1993**, *98*, 5648−5652.
(44) Grimme, S. *J. Comput. Chem.* **2006**, *27*, 1787−1799.
(45) Zhao, Y.; Truhlar, D. G. *Theor. Chem. Acc.* **2007**, *120*, 215−241.
(46) Vydrov, O. A.; Scuseria, G. E. *J. Chem. Phys.* **2006**, *125*, 234109.
(47) Chai, J.-D.; Head-Gordon, M. *Phys. Chem. Chem. Phys.* **2008**, *10*, 6615−6620.
(48) Cossi, M.; Rega, N.; Scalmani, G.; Barone, V. *J. Comput. Chem.* **2003**, *24*, 669−681.
(49) Sherwood, P.; de Vries, A. H.; Guest, M. F.; Schreckenbach, G.; Catlow, C. R. A.; French, S. A.; Sokol, A. A.; Bromley, S. T.; Thiel, W.; Turner, A. J.; Billeter, S.; Terstegen, F.; Thiel, S.; Kendrick, J.; Rogers, S. C.; Casci, J.; Watson, M.; King, F.; Karlsen, E.; Sjøvoll, M.; Fahmi, A.; Schaefer, A.; Lennartz, C. *J. Mol. Struct. (THEOCHEM)* **2003**, *632*, 1−28.
(50) Smith, W.; Forester, T. R. R. *J. Mol. Graph.* **1996**, *14*, 136−141.
(51) De Vries, A. H.; Sherwood, P.; Collins, S. J.; Rigby, A. M.; Rigutto, M.; Kramer, G. J. *J. Phys. Chem. B* **1999**, *103*, 6133−6141.
(52) Billeter, S. R. S.; Turner, A. A. J.; Thiel, W. *Phys. Chem. Chem. Phys.* **2000**, *2*, 2177−2186.
(53) Van der Kamp, M. W.; Mulholland, A. J. *Biochemistry* **2013**, *52*, 2708−2728.
(54) Lonsdale, R.; Harvey, J. N.; Mulholland, A. J. *J. Phys. Chem. Lett.* **2010**, *1*, 3232−3237.
(55) Lawan, N.; Ranaghan, K. E.; Manby, F. R.; Mulholland, A. J. *Chem. Phys. Lett.* **2014**, *608*, 380−385.
(56) Trickey, P.; Basran, J.; Lian, L.; Chen, Z.; Barton, J. D.; Sutcliffe, M. J.; Scrutton, N. S.; Mathews, F. S. *Biochemistry* **2000**, *39*, 7678−7688.

DOI: 10.1021/cs501694q
ACS Catal. 2015, 5, 1227−1239